Current Zoology, 2021, 67(4), 361–370
doi: 10.1093/cz/zoaa080
Advance Access Publication Date: 12 January 2021
Article

Article

Spatial dynamics of Chinese Muntjac related to past and future climate fluctuations

Zhonglou Sun[a,§], Pablo Orozco-terWengel[b,§], Guotao Chen[a], Ruolei Sun[a], Lu Sun[c], Hui Wang[a], Wenbo Shi[a], and Baowei Zhang[a,*]

[a]School of Life Sciences, Anhui University, Hefei, 230601, China, [b]School of Biosciences, Cardiff University, Cardiff, CF103AX, UK, and [c]Key Laboratory for Plant Diversity and Biogeography of East Asia, Kunming Institute of Botany, Chinese Academy of Sciences, Kunming, 650201, China

*Address correspondence to Baowei Zhang. E-mail: zhangbw@ahu.edu.cn.

[§]These authors contributed equally to this work.

Handling editor: Yanping Wang

Received on 26 July 2020; accepted on 16 December 2020

Abstract

Climate fluctuations in the past and in the future are likely to result in population expansions, shifts, or the contraction of the ecological niche of many species, and potentially leading to the changes in their geographical distributions. Prediction of suitable habitats has been developed as a useful tool for the assessment of habitat suitability and resource conservation to protect wildlife. Here, we model the ancestral demographic history of the extant modern Chinese Muntjac *Muntiacus reevesi* populations using approximate Bayesian computation (ABC) and used the maximum entropy model to simulate the past and predict the future spatial dynamics of the species under climate oscillations. Our results indicated that the suitable habitats for the *M. reevesi* shifted to the Southeast and contracted during the Last Glacial Maximum, whereas they covered a broader and more northern position in the Middle Holocene. The ABC analyses revealed that the modern *M. reevesi* populations diverged in the Middle Holocene coinciding with the significant contraction of the highly suitable habitat areas. Furthermore, our predictions suggest that the potentially suitable environment distribution for the species will expand under all future climate scenarios. These results indicated that the *M. reevesi* diverged in the recent time after the glacial period and simultaneously as its habitat's expanded in the Middle Holocene. Furthermore, the past and future climate fluctuation triggered the change of Chinese muntjac spatial distribution, which has great influence on the Chinese muntjac's population demographic history.

Key words: climate fluctuations, Middle Holocene, *Muntiacus reevesi*, spatial dynamics, suitable habitat

Herbivores are known to be strongly affected by environmental and subtle landscape changes, being particularly sensitive to extremely cold temperatures and dry environmental conditions (Storfer et al. 2010; Sun et al. 2019), therefore making them ideal taxa for studying how historical events affected their demographic history (Baker and Hoelzel 2014; Yannic et al. 2014; Jenkins et al. 2018). The Chinese muntjac *Muntiacus reevesi* is a small deer widely distributed in Southern China and Taiwan (Sheng et al. 1992). It is a forest-dwelling species, inhabiting mountainous terrain with good cover (Wang 1990; Sheng et al. 1992). IUCN categorizes the *M. reevesi* as of least concern (LC), however, they report a decreasing population trend throughout the species' range with their habitat being threatened due to the development of residential and commercial infrastructures, land conversion for agriculture, logging, and direct hunting (IUCN Red List 2020, https://www.iucnredlist.org/). In a previous study, the demographic history of *M. reevesi* seems to

indicate a concordance with the cycling of glacial–interglacials in late Pleistocene, whereas the recent population history having been influenced by early anthropogenic activity (Sun et al. 2019). Southern China is a biodiversity hotspot in East Asia, harboring high levels of endemism and extensive biodiversity (He and Jiang 2014). It is necessary for us to understand how climate-driven effects on *M. reevesi* spatial dynamics and its early evolutionary history. In view of the spatial dynamics, together with the population evolutionary history, we predicted that *M. reevesi* may be an ideal model mammal to test the hypotheses on how climate change can impact species distribution modeling (SDM) in Southern China.

Climate-driven range fluctuations during the Late Pleistocene have continuously shaped species distributions, diversification patterns, and demographic dynamics (Hewitt 2000; Hewitt 2004; Yannic et al. 2014). Contemporary climate change is similarly influencing species distributions and population structure, with important consequences for species' evolutionary potential (Araújo and Rahbek 2006; Parmesan 2006; Morin and Lechowicz 2008; Beever et al. 2011; Comte et al. 2013; O'Brien et al. 2013). Furthermore, human-induced environmental change and habitat fragmentation pose major threats to biodiversity and require active conservation efforts to mitigate their consequences (Cincotta et al. 2000; Condamine et al. 2013; Sievers et al. 2018; Feng et al. 2019). Therefore, identifying species vulnerable to climate change and the extent of their vulnerability is vital for guiding effective conservation efforts (Araújo and Rahbek 2006; O'Brien et al. 2013; Stanton et al. 2015). Although Southern China was not glaciated, it also experienced cooler and possibly drier climates during the Pleistocene (Williams et al. 1998; Li et al. 2004). In the context of climatic cycling, many species experienced periodic habitat expansions or contractions to meet their ecological requirements. For example, Feng et al. (2019) showed how the endangered crested ibis *Nipponia nippon* expanded its range during the Last Interglacial (LIG, ~120–140 Kya) and retracted into small refugia during the Last Glacial Maximum (LGM, ~21 Kya) whereas Zhou et al. (2016) revealed the suitable habitat of golden snub-nosed monkeys *Rhinopithecus roxellana* expanded toward warmer Southern areas during the LGM. Amphibians (Zhang et al. 2008; Blair et al. 2013; Yuan et al. 2016; Wei et al. 2020), as well as some plants (Qi et al. 2012; Tian et al. 2015; Ma et al. 2019), also exhibit such geographic range distribution changes during Late Pleistocene. However, several studies also detected unusual distribution modeling during the LGM (Yannic et al. 2014; Pan et al. 2019b).

Since the 1920s, population geneticists focus on species' population evolutionary history, their genetic structure, and how changes in their effective population sizes modify genetic variation (Templeton 1998; Condamine et al. 2013). The main aims of population genetics are to characterize the distribution of genetic variation within and among subpopulations of interbreeding organisms, to study gene flow, genetic drift, mating systems, mutation, and natural selection, etc. (Slatkin 1977; Templeton 1998; Tremblay and Ackerman 2001). With the help of modern genetic techniques, population genetics has revealed complex demographic processes (Cornuet et al. 2014; Zhao et al. 2017; Liu et al. 2018; Hu et al. 2019), as well as have helped characterizing the relationships among the alleles or haplotypes and their spatial distributions (Templeton 1998; Zhou et al. 2016; Stucki et al 2017; Wei et al. 2020). For example, using a combination of population genomic analyses, archeological records, and historical ethnic demographics data, Zhao et al. (2017) identified the genetic signatures of the origins, secondary expansions, and admixtures in Chinese sheep *Ovis aries*, thereby providing evidence about the peopling patterns of nomads and the expansion of early pastoralism in East Asia. Using a combination of whole-genome sequence data, Y-chromosomes, and mitochondrial genomes, Hu et al. (2020) provided the first comprehensive genetic evidence for species divergence and long-term population bottlenecks in red pandas *Ailurus fulgens*, demonstrating substantial interspecies genetic divergence. In addition, using expressed sequence tag–Simple Sequence Repeat (EST-SSR) nuclear markers, Erichsen et al. (2018) found that the ash *Fraxinus excelsior* population divergence between European and Hyrcanian populations was dated back to the end of the middle to Upper Pleistocene and the populations experienced a recent reduction in its effective population size. Because genetic data carries such a rich information about species old and recent evolutionary history (e.g., Aitken et al. 2008; Taubmann et al. 2011; Hu et al. 2017; Liu et al. 2018; Liao et al. 2020), embedding that information within management plans for species' conservation is likely to have a positive effect and reduce extinction rates.

In this study, we sampled *M. reevesi* along the Yangtze River and used molecular markers combined with geographic information system-based environmental niche analyses to better evaluate population genetic differentiation processes and understand how historical climate-induced species' distributional shifts. First, we used ecological niche modeling (ENM), combined with paleoclimate data to infer historical causes for the distribution pattern of *M. reevesi* as well as we used future climate predictions to define the species future distribution under different climate scenarios. Second, we used statistical phylogenetic methods to test the *M. reevesi*'s population differentiation process. The integrative analysis of population history and SDM enabled exploring the architecture of the evolutionary history and population dynamics of *M. reevesi* while shedding light on the ancient and future climate fluctuations in Southern China.

Materials and Methods

Distribution records collection, sample collection

In this study, we collected the *M. reevesi* distribution records from previously published data between 1976 and 2018 (Supplementary Table S1). If samples only had localities available, Google Earth was used to infer the coordinates of the records at the center point of the locality. Records with obvious geocoding errors were discarded, and duplicate records were removed manually. Finally, a total of 226 records of *M. reevesi* in China were collected, resulting in a detailed distribution map cover (Figure 1). What's more, 360 skin samples of *M. reevesi* were collected from 7 populations as previously described (Sun et al. 2019).

Data analysis

For forecasting the potential distribution shifts of *M. reevesi* under different climate scenarios (current, past, and future), we carried out ecological niche modelling using the MAXENT software (version 3.4.1) that is widely applied to conservation research (Phillips et al. 2006). Compared with other methods, MAXENT has higher performance, it is suitable for datasets consisting of presence-only recordings (Elith et al. 2006; Peterson et al. 2011), and it is insensitive to small sample sizes (Wisz et al. 2008). In this study, we collected all reported *M. reevesi* records, which covered nearly all habitats for this species in China. For the current climate predictions, we downloaded raster coverages of 20 environmental variables (Supplementary Table S2) from the WorldClim database (http://www.worldclim.org) at 2.5 arc-min resolution (Hijmans et al. 2005). To avoid multicollinearity of variables, we estimated the

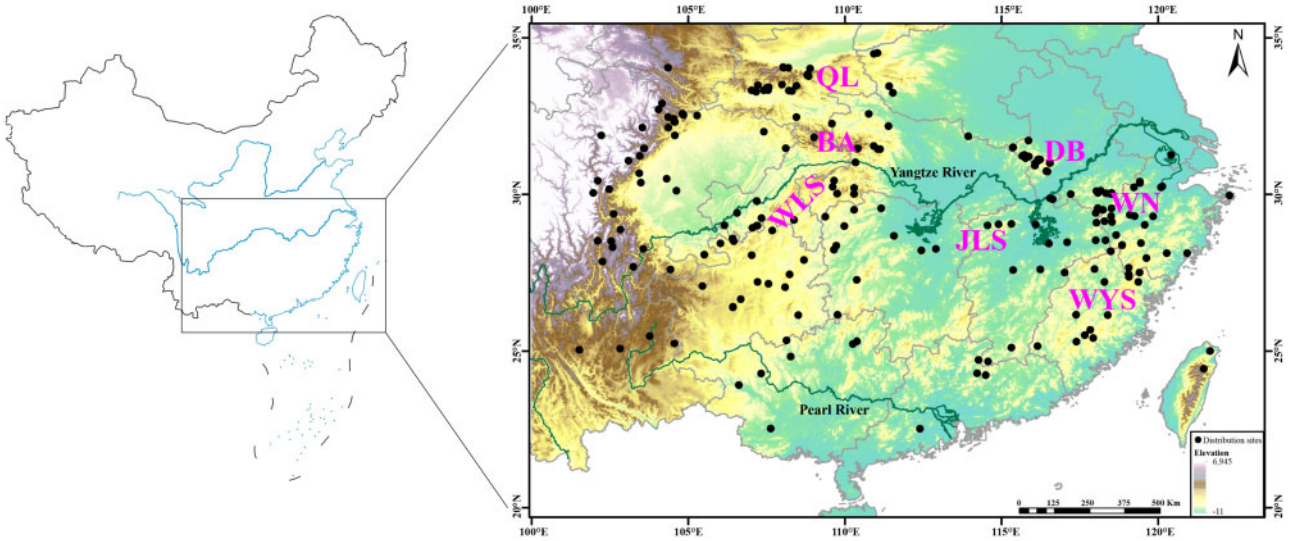

Figure 1. Map showing the distribution sites and sampling location of Chinese muntjac in Southern China. QL, Qinling Mountains; BA, Dabashan Mountains; WLS, Wulingshan Mountains; DB, Dabieshan Mountains; JLS, Jiulingshan Mountains; WN, Wannan Mountains; WYS, Wuyishan Mountains. The base maps are from Standard Map Service website (http://bzdt.ch.mnr.gov.cn/index.html).

Pearson correlation coefficients for each pair of variables and eliminated the variables with high correlation (|Pearson r| $\geq$ 0.85; Pearson 1920). Finally, out of the total 20 environmental variables, we selected a subset of 9 variables with a correlation <0.85 as predictors, including BIO1 (Annual Mean Temperature), BIO2 (Mean Diurnal Range), BIO3 (Isothermality), BIO4 (Temperature Seasonality), BIO8 (Mean Temperature of Wettest Quarter), BIO12 (Annual Precipitation), BIO15 (Precipitation Seasonality), BIO16 (Precipitation of Wettest Quarter), and Elevation. We chose MIROC5 model for the current data and the LIG, the LGM, and the Middle Holocene to obtain the predicted species distribution across time. In addition, we used the same set of bioclimatic variables collected from the WorldClim database for the LIG, LGM, and the Middle Holocene predictions. What's more, we forecast 4 alternative climatic futures based on MIROC5 and 4 representative concentration pathways (RCPs) implemented by the Intergovernmental Panel on Climate Change. These RCPs are RCP2.6 that correspond to a very stringent scenario forecasting no further increase than 2 degrees by the year 2100, based on drastic changes to CO_2, CH_4, and SO_2 emissions; RCP4.5 that corresponds to an intermediate scenario whereby temperature may increase between 2 and 3 degrees by 2100 based on the start of the decline of the 3 greenhouse gases mentioned before by 2050; RCP6.0 which considers that greenhouse gas emission will start to decline around 2080 and RCP8.5 which is considered to be the worse warming up scenario with emissions not declining throughout the 21st century (Remya et al. 2015).

For each climatic scenario, we randomly divided distribution data into training data (80%) and validation data (20%) and run 50 replications using the subsampling method. The maximum number of background points was set to 10,000, and the maximum iterations were set to 5,000 times for seeking the optimal solution (Phillips et al. 2006; Hazzi et al. 2018; Liao et al. 2020), whereas we used for the remaining parameters default values. The maximum training sensitivity plus specificity threshold (MTSS) maximizes the proportions of correctly identified positives and correctly identified negatives and is considered to predict presence/absence most accurately (Jiménez-Valverde and Lobo 2007). In this study, we reclassified the suitability layer into 4 classes: unsuitable habitat (<MTSS), minimally suitable habitat (MTSS—0.3), moderately suitable habitat (0.3–0.6), and highly suitable habitat (>0.6) as Liao et al. (2020) recommended. Model performance under each climatic scenario was assessed by the area under the curve (AUC) of receiver operating characteristics (Hanley and McNeil 1982) and true skills statistics (TSS; Allouche et al. 2006). If the values of AUC and TSS close to 1, that indicates the model performed excellent, whereas the AUC value <0.5 or the TSS value close to 0 means that it fails to describe reality (Swets 1988; Allouche et al. 2006).

In this study, all microsatellite genotyping data were derived from Sun et al. (2019). Micro-Checker was used to detect the presence of null alleles and genotyping errors in microsatellite genotyping (Van Oosterhout et al. 2004). Deviation from Hardy–Weinberg equilibrium for each locus and for all loci for each population was evaluated using exact probability tests implemented in GenePop v.4.2.1 (Rousset 2008). The same software was used to test for the presence of linkage disequilibrium within each of the populations. Pairwise divergence between populations was estimated with Microsatellite Analyzer (Dieringer and Schlötterer 2003) using 10,000 permutations to determine significance. The presence of population structure was determined using STRUCTURE (Pritchard et al. 2000) ran for values of the number of clusters (K) in the data from 1 until 7, with STRUCTURE ran 5 times for each value of K. A total of 10^6 steps of STRUCTURE's Markov Chain Monte Carlo algorithm were run with additional 10^4 steps as burn-in. The most suitable clustering solution was determined using Evano's method (Evanno et al. 2005) as implemented in StructureHarvester (Earl and vonHoldt 2012).

Approximate Bayesian computation (ABC) was used to estimate the fit of 2 alternative scenarios that could explain the demographic history of the 7 populations of *M. reevesi*. Each scenario had the same prior probability (i.e., 50%). In one of them, the 7 populations passed through a population bottleneck sometime within the last 10,000 years as suggested by Sun et al. (2019) after which their *Ne* (effective population size) was free to vary, and in the other scenario no bottleneck constraint was imposed. The fit of the 2 scenarios to the observed data was determined with a logistic regression as

implemented in DIY-ABC, and the most suitable model was used to estimate demographic parameters for the 7 populations (*Ne*) and the time of divergence between pairs of populations. A total of 100,000 simulations were carried out for each scenario. The divergence pattern between populations was determined based on the *F*st estimates of the pairwise population divergence. This consisted of a tree with a deep divergence splitting the samples into 2 branches, with 1 branch including the QL, BA, and WLS populations, and the other one including the DB, JLS, WN, and WYS populations (Figure 2A), in line with previous Structure result (Figure 2B, Sun et al. 2019). This analysis was carried out in DIY-ABC 2.1.0 (Cornuet et al. 2014) with 1 million simulations to estimate the posterior distribution for each of the populations' *Ne* and the times of divergence. Wide uniform prior distributions (where all numbers between the smallest and the largest number of the range have the same probability; Durrett 1999) for each parameter were used with the prior range for the *Ne* values ranging between 10 and 400,000, and for the times of divergence between 10 and 30,000 years ago (Supplementary Table S3). The simulations generated in DIY-ABC followed default parameters for the mutation model for microsatellites implemented in DIY-ABC. The simulations were summarized with the mean number of alleles per locus and mean genetic diversity measured in each simulated population separately as well as measured on all combined pairs of populations, and with the pairwise *F*st measured between all pairs of populations. The posterior distribution of each parameter was estimated using the 1% closest simulations to the observed data.

Results

Historical dynamics of distributions

The ENMs had excellent predictive power for occurrences under conditions of the Current, the Holocene (8–4 Ka), the LGM (29–11 Ka), and the LIG (140–120 Ka). The AUC had values >0.85 in all analyses, which implied that the results greatly differed from random prediction (AUC = 0.5; Supplementary Table S4). What's more, TSS results showed similar tendency and suggest that all model outputs also with no random effect (Supplementary Table S4). For *M. reevesi*, suitable habitats presently occurred in Southern China (Figure 1). Compared with the LIG, the LGM MAXENT projection predicted more narrow habitat hotspots and shifted them to China's Southeast (Figure 3A and B). Furthermore, the Middle Holocene MAXENT projection predicted a broader distribution, which *M. reevesi* potentially having dispersed to the North of China (Figure 3C). Today, our simulations predict a similar continuous distribution compared with the Middle Holocene area, but some differences existed for the most suitable areas (Figure 3D).

Future potentially suitable climatic distribution

The predicted future (the 2050s) suitable habitat distributions of *M. reevesi* under RCP 2.6, RCP 4.5, RCP 6.0, and RCP 8.5 climate change scenarios are shown in Figure 4. We also obtained high AUC and TSS values for each climate scenario, suggesting model performance of ENM is reliable (Supplementary Table S4). Compared with

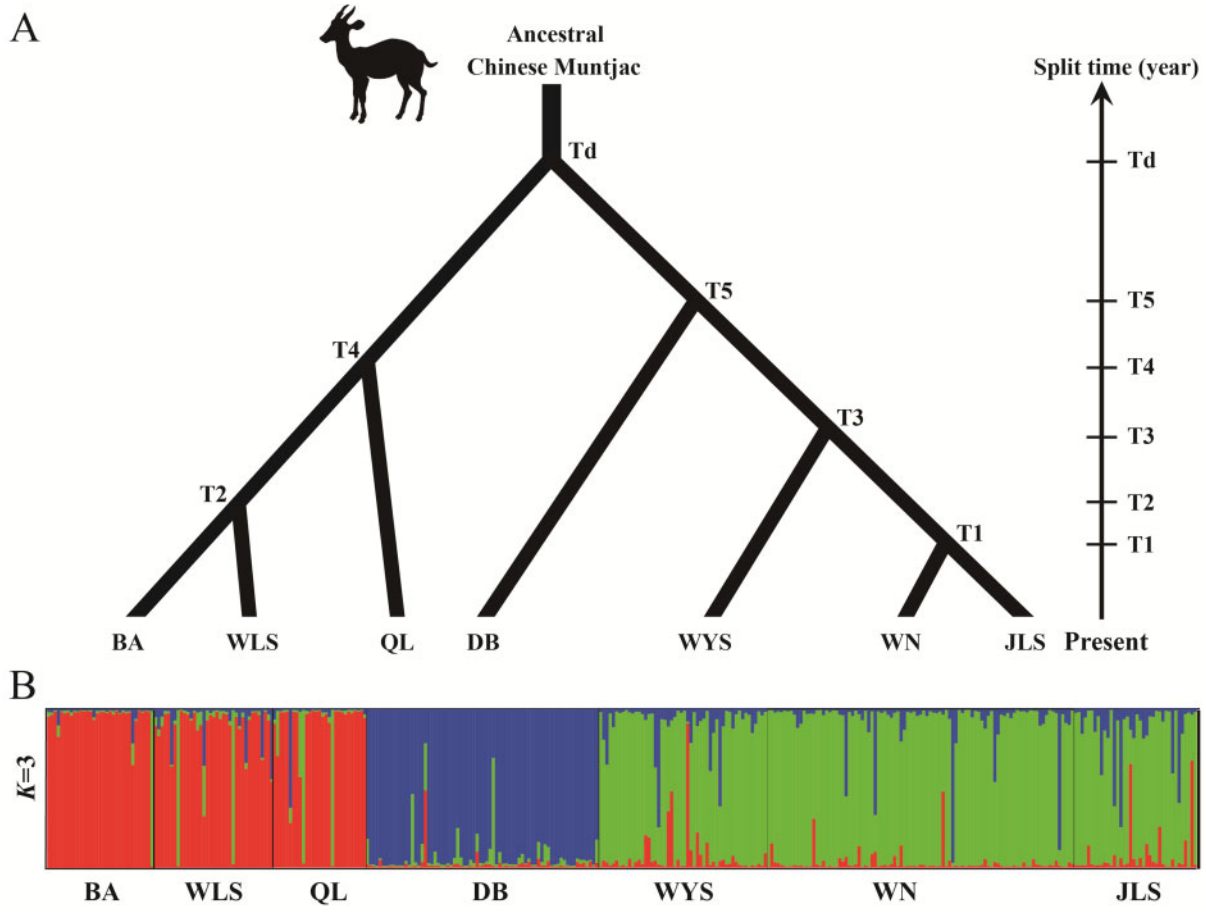

Figure 2. Divergence patterns used for the DIY-ABC simulations (**A**), and Bayesian STRUCTURE clustering among Chinese muntjac populations (**B**). The bottom Bayesian STRUCTURE clustering results of microsatellite variation among 7 Chinese muntjac populations at $K = 3$ were derived from Sun et al. (2019).

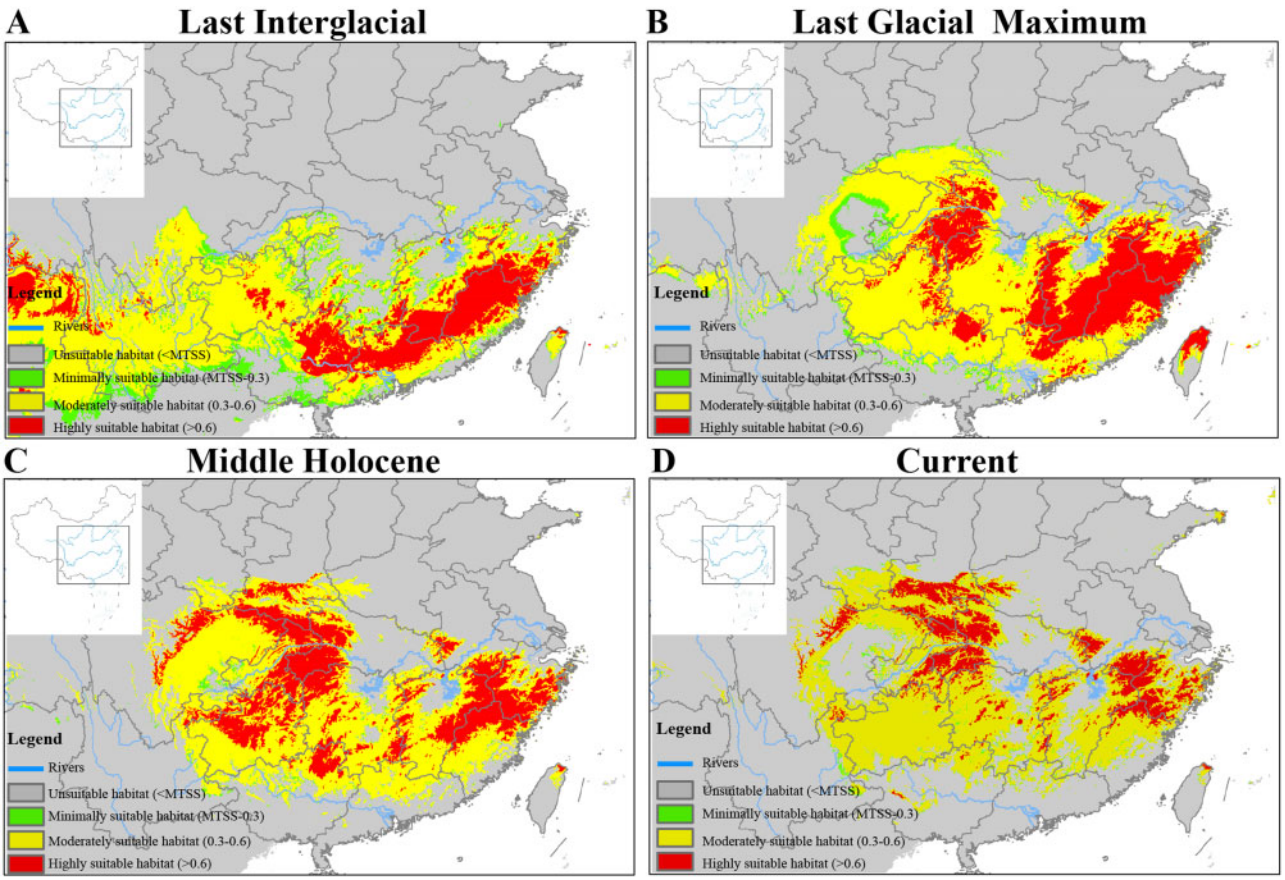

Figure 3. Species distribution models of Chinese muntjac at (**A**) the Last Interglacial, (**B**) the Last Glacial Maximum, (**C**) the Middle Holocene, and (**D**) the Current. Color scale refers to probability of habitat suitability as predicted by MAXENT. The base maps are from Standard Map Service website (http://bzdt.ch.mnr.gov.cn/index.html).

the current distribution, in the 2050s, the total area of the unsuitable habitat regions for *M. reevesi* under the 4 RCPs (RCP 2.6, RCP 4.5, RCP 6.0, and RCP 8.5) would decrease by 6.95, 5.19, 6.51, and 8.5%, respectively (Table 1), and the total area of the minimally suitable regions would increase by 5.02, 4.73, 5.94, and 3.49%, respectively (Table 1). Meanwhile, the total area of the moderately suitable regions for *M. reevesi* would increase by 2, 1.06, 0.9, and 3.14%, respectively (Table 1). Under scenario RCP 8.5, the area of the highly suitable regions would increase by 1.87%, whereas under scenario RCP 2.6, RCP 4.5, and RCP 6.0, the areas of the highly suitable regions would decrease by 0.07, 0.6, and 0.32% (Table 1).

Demographic reconstruction

The demographic scenario comparison between a model including a bottleneck versus one without it and with both models having the same prior probability, showed that the model without a bottleneck fitted the observed data substantially better (no bottleneck scenario: probability 0.99–95% confidence interval (CI) 0.991–0.997; bottleneck scenario: probability 0.0059–95% CI 0.0029–0.0089). We estimated the recent demographic history of the 7 *M. reevesi* populations based on the scenario without forcing a bottleneck in the populations' recent history (Table 2). Overall, this scenario indicates that the posterior distribution of the ancestral population to the 7 modern *M. reevesi* population was characterized by a *Ne* mode of 751 (95% Highest Posterior Density [HPD] 346–41,900) whereas its derived populations presented substantially larger *Ne* posterior distributions values with modes ranging between 16,400 and 275,000, and with the mode of posterior distribution of the divergence age between the 2 main groups of populations at 10,400 years ago (95% HPD 4,180–27,900 years ago; Table 3, Figure 5). Overall, the effective population size of posterior distributions South populations (JLS, WN, and WYS; 16,400–59,200) was much smaller than those of the North (QL, BA, WLS, and DB; 57,800–275,000; Table 2, Figure 5). The divergences between pairs of populations in the DB, JLS, WN, and WYS cluster had the modes of their posterior distributions ranging between 1,660 and 7,220 years ago, while those for the QL, BA, and WLS cluster it ranged between 2,680 and 4,690 years ago (Table 3, Figure 5). Overall, the divergence between the modern *M. reevesi* was dated back to the Middle Holocene.

Discussion

The Chinese muntjac is widely distributed in Southern China, typically inhabiting temperate forests with occasional snowfall, as well as dense forests in the warm subtropical zone (Wang 1990; Sheng et al. 1992). In this study, the ENM revealed that the suitable habitat areas for *M. reevesi* significantly changed in the Late Pleistocene. Particularly, the species' highly suitable habitats were mainly distributed in Southern China and in Northern Myanmar during the LIG (140–120 Ka, Figure 3A), whereas they shifted to Southeast China during the LGM (29–11 Ka, Figure 3B). In the Middle Holocene (8 Ka–4 Ka), the suitable habitats for the *M. reevesi* were much

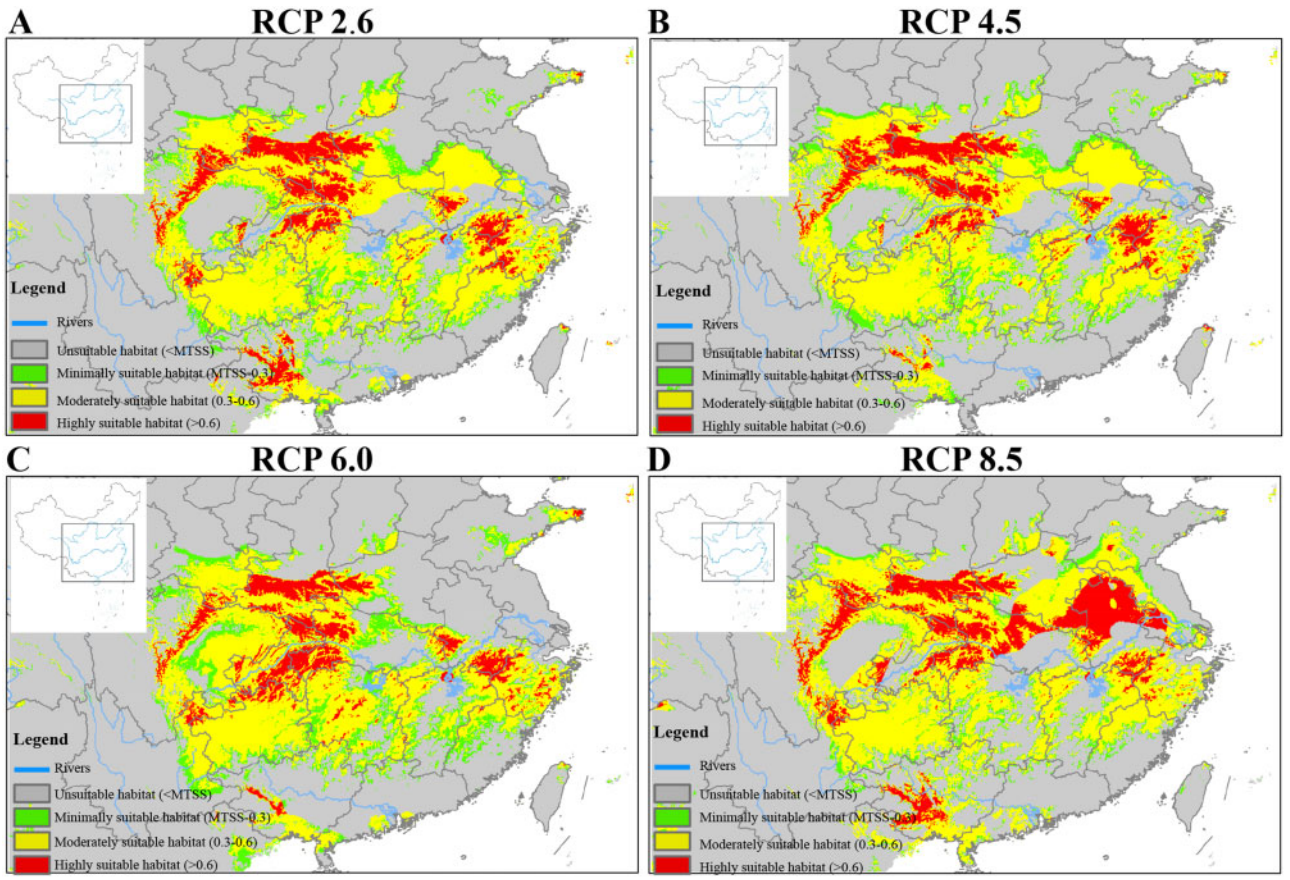

Figure 4. Species distribution models of Chinese muntjac predicted in the 2050s under 4 emission scenarios (**A**) RCP 2.6, (**B**) RCP 4.5, (**C**) RCP 6.0, and (**D**) RCP 8.5. Color scale refers to probability of habitat suitability as predicted by MAXENT. The base maps are from Standard Map Service website (http://bzdt.ch.mnr.gov.cn/index.html).

Table 1. Predicted distribution for Chinese muntjac under current and future climatic conditions

Decades	scenarios	Predicated distribution (cells)				Increased/decreased rate (%)			
		Unsuitable habitat	Minimally suitable habitat	Moderately suitable habitat	Highly suitable habitat	Unsuitable habitat	Minimally suitable habitat	Moderately suitable habitat	Highly suitable habitat
Current	/	198,201	2,127	48,869	13,129	/	/	/	/
2050s	RCP2.6	179,979	15,289	54,124	12,934	−6.95	5.02	2.00	−0.07
	RCP4.5	184,587	14,536	51,652	11,551	−5.19	4.73	1.06	−0.6
	RCP6.0	181,122	17,710	51,224	12,270	−6.51	5.94	0.90	−0.32
	RCP8.5	175,898	11,292	57,114	18,022	−8.50	3.49	3.14	1.87

Notes: Number of spatially defined cells under different scenarios at a resolution of 2.5 arc-min × 2.5 arc-min. The increased/decreased rate was compared with the current distribution.

broader than ever including parts of Northern China (Figure 3C); however, following that period of time, these habitats started contracting until finally reaching the current distribution (Figure 3D). Previous studies in other Asiatic species have also shown that despite having formally extensive ranges, their suitable niches contracted during the change from the LIG to the LGM, for example, the crested ibis (*N. nippon*, Feng et al. 2019) and the Jerdon's tree frog *Hyla annectans* (Wei et al. 2020). A similar observation but with a drastic shift of the distribution range toward the south has been described for the golden snub-nosed monkey *R. roxellana* (Zhou et al. 2016), whereas some amphibians *Microhyla fissipes* complex (Yuan et al. 2016) and *Odorrana graminea* (Chen et al. 2020) presented extensive range during the LGM in Southern China. Compared with the LIG, the temperature and precipitation declined rapidly during the LGM (Shi et al. 2008; Zhao et al. 2011). Particularly, in Southern China, the temperature reduced by 6°C–7°C and precipitation decreased by 400–600 mm/year during the LGM (Zhou et al. 1991). In consistence with these changes, it was been shown that most vegetation ranges contracted and shifted to the south during the LGM (Wang et al. 2019), whereas during the Holocene forests expanded and the climate became moistier, particularly toward the middle Holocene (Zhao and Yu 2012). As a

typical forest-dwelling species, the *M. reevesi* is very sensitive to cold temperatures and dry environmental conditions (Sun et al. 2019). During the Pleistocene, climatic fluctuations had important effects on biodiversity and changes in the geographic distribution of mammals (He and Jiang 2014; He et al. 2016; Zhou et al. 2016). Therefore, it is likely that the cold weather in the LGM triggered the *M. reevesi* hotspots habitat contraction and shift to the Southeast, whereas the more comfortable environment in the Middle Holocene broadened the habitat hotspots for the *M. reevesi*.

Sun et al. (2019) revealed that the relative warmer weather in the LIG triggered *M. reevesi* population expansion, whereas the cold weather in the LGM induced a severe population decline. Nevertheless, the Bayesian Skyline Plot analysis by Sun et al. (2019) reveals a rapid demographic expansion starting ~8,000–7,000 years ago that is consistent with our demographic analyses results that suggest the extant *M. reevesi* populations derive from an ancestral small population. Previous studies also showed that other Southern China mammals experienced recent population decline events, which may have been triggered by the increase in early human activities in the region during the Holocene (Zhang et al. 2007; Hu et al. 2011; Sun et al. 2016; Sun et al. 2019). However, in this study, we found the *M. reevesi* habitat shifted and contracted significantly since the Middle Holocene (Figure 3C and D). Therefore, we speculated that the climate fluctuations induced habitat shifting or contraction may have had a greater influence than the early human activities on recent population decline events.

In this study, the demographic reconstruction analysis revealed that the modern *M. reevesi* grouped into 3 main genetic clusters (QL/BA/WLS, DB, and JLS/WN/WYS), which diverged in the Middle Holocene (Figure 5). In Southern China, population

Table 2. Demographic parameters inferred with DIY-ABC

	Mode	5% HPD LB	95% HPD UB
QL	22100.00	8850.00	36500.00
BA	16400.00	5090.00	36600.00
WLS	59200.00	29300.00	77400.00
DB	28300.00	14600.00	38300.00
JLS	109000.00	51700.00	194000.00
WN	57800.00	20500.00	77800.00
WYS	275000.00	93500.00	1410000.00
Ancestral population	751.00	346.00	41900.00

Notes: The model of the posterior distribution of each parameter is shown in the column Mode, with the 2 adjacent columns presenting the lower bound of the 95% HPD of the distribution (5% HPD LB) and the corresponding upper bound (95% HPD UB). Parameter names are shown in Figure 5.

Table 3. Divergence parameters inferred with DIY-ABC

	Mode	5% HPD LB	95% HPD UB
T1	1660.00	268.00	6950.00
T2	3880.00	924.00	9360.00
T3	7220.00	3230.00	14300.00
T4	2680.00	579.00	11100.00
T5	4690.00	2170.00	17500.00
Td	10400.00	4180.00	27900.00

Notes: The model of the posterior distribution of each parameter is shown in the column mode, with the 2 adjacent columns presenting the lower bound of the 95% HPD of the distribution (5% HPD LB) and the corresponding upper bound (95% HPD UB). Parameters are also shown in Figure 5.

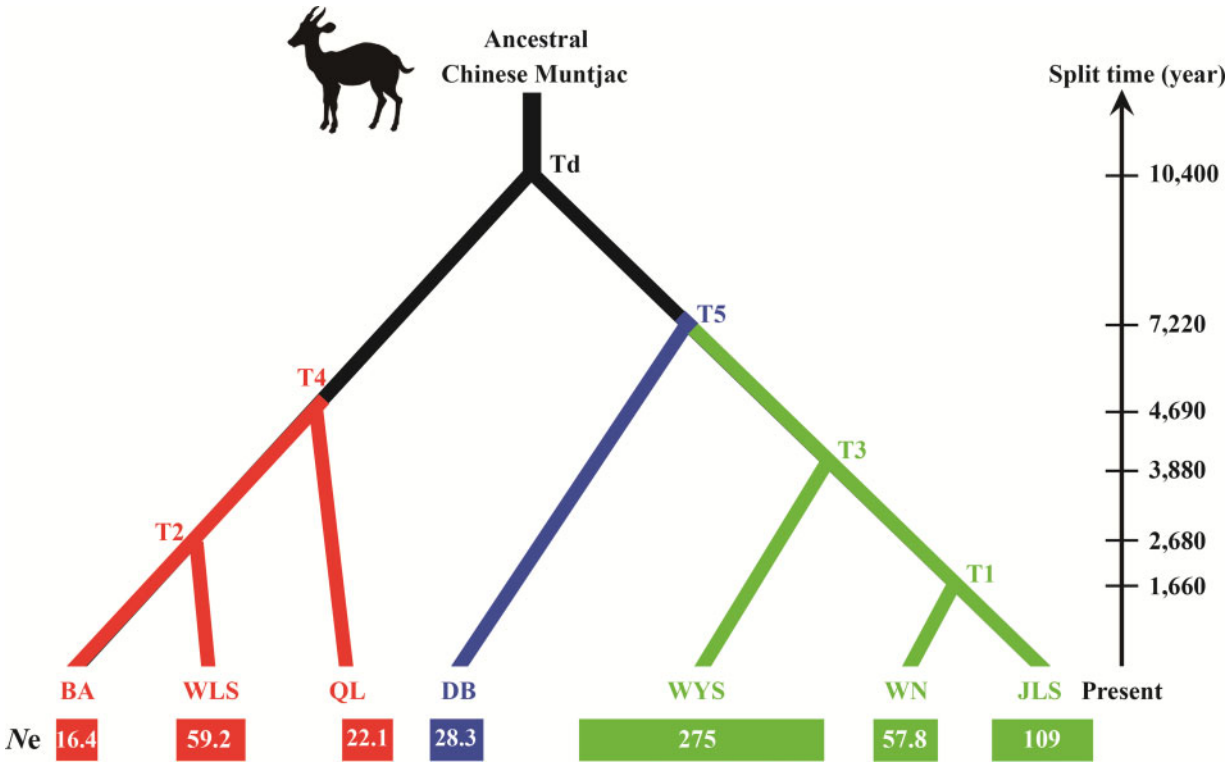

Figure 5. The inferred divergence time and demographic history of Chinese muntjac populations in Southern China with DIY-ABC. The bottom rectangles represent the population size of each population, and the number in the rectangles is the effective population size (*Ne*, unit: 1,000).

divergence events also happened in the recent time as observed in the giant panda *Ailuropoda melanoleuca* (Zhao et al. 2013), the snub-nosed monkeys *Rhinopithecus* spp. (Zhou et al. 2016), the brown Norway rats *Rattus norvegicus* (Teng et al. 2017), and the red panda *A. fulgens* (Hu et al. 2020). The ENM analysis showed that the suitable habitat for the *M. reevesi* covered a much broader region than ever thought, and that it may have migrated to the North in the Middle Holocene as suitable habitat became available (Figure 3C). Therefore, we hypothesized that the *M. reevesi* populations diverged with the expansion of their habitats' area. Among 7 populations, the DB population from the Dabie Mountains diverged first ~7,220 years ago and formed an independent cluster that was closer to the JLS/WN/WYS (Figure 5). The uniqueness of the DB *M. reevesi* population is not surprising considering their occurrence in the Dabie Mountains. Located at mid-latitude in East Asia, the Dabie Mountains are composed of a chain of ancient, isolated, low-middle elevation massifs (Pan et al. 2019b). Furthermore, the Dabie Mountains are in the ecotone of subtropical evergreen broad-leaved forest and the warm-temperate deciduous broad-leaved forest zone, with annual average temperature of 12.5°C and mean annual precipitation of 1,832.8 mm (Zheng et al. 2012). In recent decades, several new species were discovered in Dabie Mountains in various taxonomic groups including mammals (e.g., Anhui Musk Deer, *Moschus anhuiensis*, Li et al. 1999), reptiles (e.g., Dabie Mountains Pit Viper, *Protobothrops dabieshanensis*, Huang et al. 2012; Zhang et al. 2013), and amphibians (e.g., Anhui Tree Frog, *Rhacophorus zhoukaiyae*, Pan et al. 2017; Dabie Mountain Brown Frog, *Rana dabieshanensis*, Wang et al. 2017; Anhui Knobby Newt, *Tylototriton anhuiensis*, Qian et al. 2017). Furthermore, Pan et al. (2019a) presented evidence that multiple hidden species exist in the genus *Pachyhynobius*, which presents a narrow habitat distribution across this mountain range. Together these findings strongly suggest that species endemic to the Dabie Mountains correspond to distinct lineages and the DB *M. reevesi* falls within this category. What's more, we think that the isolated massifs in this mountain range, present more comfortable and stable climate environments that may facilitate their continuous inhabitation throughout climatic changes, which likely has contributed to exacerbating differences between lineages.

Our predictions showed that the potentially suitable climatic distribution for *M. reevesi* would expand under all future climate scenarios (RCP 2.6, RCP 4.5, RCP 6.0, and RCP 8.5; Table 1), indicating that more suitable habitats would be available for the *M. reevesi* in the future. Furthermore, this change was more obvious in the high greenhouse gas concentration scenarios (RCP 8.5) than in the low greenhouse gas concentration scenarios (RCP2.6, RCP4.5, and RCP 8.5; Figure 4, Table 1). Overall, the suitable habitats for *M. reevesi* would expand potentially enabling migration to the north in the future. However, studies have shown that different species habitat's respond differently to climate change, for example, the spatial distributions of habitat for the Golden bowerbird *Prionodura newtonia* would decrease under different future scenarios (Hilbert et al. 2004), whereas the beaded lizard *Heloderma horridum* (Domíguez-Vega et al. 2012) and the white-lipped deer *Przewalskium albirostris* (Cui et al. 2018) habitats are predicted to increase, and for other species, no appreciable habitable range changes are forecasted (e.g., Chinese Skink, *Eumeces chinensis*; Yang et al. 2020). Previous studies had concluded that global warming would greatly influence species distributions by causing expansions, shifts, or contractions in the species ranges both in vertebrates and plants (Thomas et al. 2004; Domíguez-Vega et al. 2012; Yi et al. 2016; Cui et al. 2018; Newbold 2018; Wei et al. 2018). For *M. reevesi*, future warmer climates are likely to result in an increase of vegetation in currently unhabitable areas (VanDerWal et al. 2013; Liao et al. 2020) suggesting that increased suitable habitats may further guarantee the species survival into the future, and leaving as main threats for the species habitat degradation due to logging and wood harvesting, land conversion for agriculture and urbanization, along with hunting.

In this study, our results revealed that the modern *M. reevesi* populations diverged in the Middle Holocene, thus should be treated as 3 independent management units to maintain their distinct genetic variation, and considering the DB population as a separate evolutionarily significant unit from the other 2 groups. What's more, the ENM analysis showed that the past distribution of *M. reevesi* was strongly susceptible to climate change and that the species' habitat response to the current and forecasted climate change is likely to result in a net suitable habitat increase. Therefore, we think that priority should be given to the conservation and restoration of *M. reevesi* current habitat to better maintain the species population sizes and at the same time benefit other Southern China mammals.

Acknowledgments

The authors would like to thank Liu Yang and Xuyu Wang for their help in distribution records collection. We would also like to thank Dr. Chunlin Li, Dr. Tao Pan, and 2 anonymous reviewers for providing helpful advice on the early manuscript preparation.

Funding

This work was funded by the Key Science and Technology Financing Projects of the Ministry of Education (2012), the Scientific Research and Protection Project of Black Muntjac in Qianjiangyuan National Park, Zhejiang, China (2019–2021), the Biodiversity Survey, Monitoring and Assessment Project of Ministry of Ecology and Environment, China (Grant No. 2019HB2096001006), and the National Science & Technology Fundamental Resources Investigation Program of China (Grant No. 2019FY101803).

Authors' Contributions

Z.S. and B.Z. conceived and designed the study. Z.S., G.C., R.S., W.S., and H.W. collected the data. Z.S., P.O.t.W., and L.S. analyzed the data. Z.S., P.O.t.W., and B.Z. led the writing. All authors have read and approved the manuscript for submission.

Supplementary Material

Supplementary material can be found at https://academic.oup.com/cz.

Conflict of Interest

The authors declare that they have no conflict of interest.

References

Aitken SN, Yeaman S, Holliday JA, Wang TL, Curtis-McLane S, 2008. Adaptation, migration or extirpation: climate change outcomes for tree populations. *Evol Appl* **1**:95–111.

Allouche O, Tsoar A, Kadmon R, 2006. Assessing the accuracy of species distribution models: prevalence, kappa and the true skill statistic (TSS). *J Appl Ecol* **43**:1223–1232.

Araújo MB, Rahbek C, 2006. How does climate change affect biodiversity? *Science* **313**:1396–1397.

Baker KH, Hoelzel AR, 2014. Influence of Holocene environmental change and anthropogenic impact on the diversity and distribution of roe deer. *Heredity* **112**:607–615.

Beever EA, Ray C, Wilkening JL, Brussard PF, Mote PW, 2011. Contemporary climate change alters the pace and drivers of extinction. *Glob Change Biol* **17**:2054–2070.

Blair C, Davy CM, Ngo A, Orlov NL, Shi HT et al., 2013. Genealogy and demographic history of a widespread amphibian throughout Indochina. *J Hered* **104**:72–85.

Chen Z, Li HY, Zhai XF, Zhu YJ, He YX et al., 2020. Phylogeography, speciation and demographic history: contrasting evidence from mitochondrial and nuclear markers of the *Odorrana graminea* sensu lato (Anura, Ranidae) in China. *Mol Phylogenet Evol* **144**:106701.

Cincotta RP, Wisnewski J, Engelman R, 2000. Human population in the biodiversity hotspots. *Nature* **404**:990–992.

Comte L, Buisson L, Daufresne M, Grenouillet G, 2013. Climate-induced changes in the distribution of freshwater fish: observed and predicted trends. *Freshw Biol* **58**:625–639.

Condamine FL, Rolland J, Morlon H, 2013. Macroevolutionary perspectives to environmental change. *Ecol Lett* **16**:72–85.

Cornuet JM, Pudlo P, Veyssier J, Dehne-Garcia A, Gautier M et al., 2014. DIYABC v2. 0: a software to make approximate bayesian computation inferences about population history using single nucleotide polymorphism, DNA sequence and microsatellite data. *Bioinformatics* **30**:1187–1189.

Cui SP, Luo X, Li CW, Hu HJ, Jiang ZG, 2018. Predicting the potential distribution of white-lipped deer using the maxent model. *Biodivers Sci* **26**: 171–176.

Dieringer D, Schlötterer C, 2003. Microsatellite analyser (MSA): a platform independent analysis tool for large microsatellite data sets. *Mol Ecol Notes* **3**:167–169.

Domíguez-Vega H, Monroy-Vilchis O, Balderas-Valdivia CJ, Gienger C, Ariano-Sánchez D, 2012. Predicting the potential distribution of the beaded lizard and identification of priority areas for conservation. *J Nat Conserv* **20**:247–253.

Durrett R, 1999. *Essentials of Stochastic Processes*. New York: Springer.

Earl DA, vonHoldt BM, 2012. Structure harvester: a website and program for visualizing structure output and implementing the evanno method. *Conserv Genet Resour* **4**:359–361.

Elith J, Graham CH, Anderson RP, Dudík M, Ferrier S et al., 2006. Novel methods improve prediction of species' distributions from occurrence data. *Ecography* **29**:129–151.

Erichsen EO, Budde KB, Sagheb-Talebi K, Bagnoli F, Vendramin GG et al., 2018. Hyrcanian forests-Stable rear-edge populations harbouring high genetic diversity of *Fraxinus excelsior*, a common European tree species. *Divers Distrib* **24**:1521–1533.

Evanno G, Regnaut S, Goudet J, 2005. Detecting the number of clusters of individuals using the software structure: a simulation study. *Mol Ecol* **14**: 2611–2620.

Feng SH, Fang Q, Barnett R, Li C, Han SJ et al., 2019. The genomic footprints of the fall and recovery of the crested ibis. *Curr Biol* **29**:340–349.

Hanley JA, McNeil BJ, 1982. The meaning and use of the area under a receiver operating characteristic (ROC) curve. *Radiology* **143**:29–36.

Hazzi NA, Moreno JS, Ortiz-Movliav C, Palacio RD, 2018. Biogeographic regions and events of isolation and diversification of the endemic biota of the tropical Andes. *Proc Natl Acad Sci USA* **115**:7985–7990.

He K, Hu NQ, Chen Li JT, Jiang XL, 2016. Interglacial refugia preserved high genetic diversity of the Chinese mole shrew in the mountains of southwest China. *Heredity* **116**:23–32.

He K, Jiang XL, 2014. Sky islands of southwest China. I: an overview of phylogeographic patterns. *Chin Sci Bull* **59**:585–597.

Hewitt GM, 2000. The genetic legacy of the Quaternary ice ages. *Nature* **405**: 907–913.

Hewitt GM, 2004. Genetic consequences of climatic oscillations in the Quaternary. *Philos Trans R Soc Lond B Biol Sci* **359**:183–195.

Hijmans RJ, Cameron SE, Parra JL, Jones PG, Jarvis A, 2005. Very high resolution interpolated climate surfaces for global land areas. *Int J Climatol Int J Climatol* **25**:1965–1978.

Hilbert DW, Bradford M, Parker T, Westcott DA, 2004. Golden bowerbird (*Prionodura newtonia*) habitat in past, present and future climates: predicted extinction of a vertebrate in tropical highlands due to global warming. *Biol Conserv* **116**:367–377.

Hu XJ, Yang J, Xie XL, Lv FH, Cao YH et al., 2019. The genome landscape of Tibetan sheep reveals adaptive introgression from argali and the history of early human settlements on the Qinghai–Tibetan Plateau. *Mol Biol Evol* **36**: 283–303.

Hu YB, Guo Y, Qi DW, Zhan XJ, Wu H et al., 2011. Genetic structuring and recent demographic history of red pandas (*Ailurus fulgens*) inferred from microsatellite and mitochondrial DNA. *Mol Ecol* **20**:2662–2675.

Hu YB, Thapa A, Fan HZ, Ma TX, Wu Q et al., 2020. Genomic evidence for two phylogenetic species and long-term population bottlenecks in red pandas. *Sci Adv* **6**:eaax5751.

Hu YB, Wu Q, Ma S, Ma TX, Shan L et al., 2017. Comparative genomics reveals convergent evolution between the bamboo-eating giant and red pandas. *Proc Natl Acad Sci USA* **114**:1081–1086.

Huang X, Pan T, Han DM, Zhang L, Hou YX et al., 2012. A new species of the genus *Protobothrops* (Squamata: viperidae: crotalinae) from the Dabie mountains, Anhui, China. *Asian Herpetol Res* **3**:213–218.

IUCN, 2020. *IUCN Red List of Threatened Species*. Glan, Switzerland and Cambridge. Available from: http://www.iucnredlist.org (Accessed 25 June, 2020).

Jenkins DA, Yannic G, Schaefer JA, Conolly J, Lecomte N, 2018. Population structure of caribou in an ice-bound archipelago. *Divers Distrib* **24**: 1092–1108.

Jiménez-Valverde A, Lobo JM, 2007. Threshold criteria for conversion of probability of species presence to either–or presence–absence. *Acta Oecol* **31**:361–369.

Li JJ, Shu Q, Zhou SZ, Zhang J, 2004. Review and prospects of Quaternary glaciation research in China. *J Glaciol Geocryol* **26**:235–243.

Li M, Li YG, Sheng HL, Tamate H, Masuda R et al., 1999. The re-study of the classification of *Moschus moschiferus anhuiensis*. *Chin Sci Bull* **44**: 188–192.

Liao ZY, Zhang L, Nobis MP, Wu XG, Pan KW et al., 2020. Climate change jointly with migration ability affect future range shifts of dominant fir species in Southwest China. *Divers Distrib* **26**:352–367.

Liu ZJ, Tan XX, Orozco-terWengel P, Zhou XM, Zhang LY et al., 2018. Population genomics of wild Chinese rhesus macaques reveals a dynamic demographic history and local adaptation, with implications for biomedical research. *GigaScience* **7**:giy106.

Ma XG, Wang ZW, Tian B, Sun H, 2019. Phylogeographic analyses of the East Asian endemic genus *Prinsepia* and the role of the East Asian monsoon system in shaping a North-South divergence pattern in China. *Front Genet* **10**: 128.

Morin X, Lechowicz MJ, 2008. Contemporary perspectives on the niche that can improve models of species range shifts under climate change. *Biol Lett* **4**:573–576.

Newbold T, 2018. Future effects of climate and land-use change on terrestrial vertebrate community diversity under different scenarios. *Proc R Soc B Biol Sci* **285**:20180792.

O'Brien SM, Gallucci VF, Hauser L, 2013. Effects of species biology on the historical demography of sharks and their implications for likely consequences of contemporary climate change. *Conserv Genet* **14**:125–144.

Pan T, Sun ZL, Lai XL, Orozco-terWengel P, Yan P et al., 2019a. Hidden species diversity in *Pachyhynobius*: a multiple approaches species delimitation with mitogenomes. *Mol Phylogenet Evol* **137**:138–145.

Pan T, Wang H, Orozco-terWengel P, Hu CC, Wu GY et al., 2019b. Long-term sky islands generate highly divergent lineages of a narrowly distributed stream salamander (*Pachyhynobius shangchengensis*) in mid-latitude mountains of East Asia. *BMC Evol Biol* **19**: 1.

Pan T, Zhang YN, Wang H, Wu J, Kang X et al., 2017. A new species of the genus *Rhacophorus* (Anura: Rhacophoridae) from Dabie Mountains in East China. *Asian Herpetol Res* **8**:1–13.

Parmesan C, 2006. Ecological and evolutionary responses to recent climate change. *Annu Rev Ecol Evol Syst* **37**:637–669.

Pearson K, 1920. Notes on the history of correlation. *Biometrika* **13**:25–45.

Peterson AT, Soberon J, Pearson RG, Anderson RP, Martínez-Meyer E et al., 2011. *Ecological Niches and Geographic Distributions (MPB-49)*. Princeton (NJ): Princeton University Press.

Phillips SJ, Anderson RP, Schapire RE, 2006. Maximum entropy modeling of species geographic distributions. *Ecol Model* **190**:231–259.

Pritchard JK, Stephens M, Donnelly P, 2000. Inference of population structure using multilocus genotype data. *Genetics* **155**:945–959.

Qi XS, Chen C, Comes HP, Sakaguchi S, Liu YH et al., 2012. Molecular data and ecological niche modelling reveal a highly dynamic evolutionary history of the East Asian Tertiary relict *Cercidiphyllum* (Cercidiphyllaceae). *New Phytol* **196**:617–630.

Qian LF, Sun XN, Li JQ, Guo WB, Pan T et al., 2017. A new species of the genus *Tylototriton* (Amphibia: urodela: salamandridae) from the southern Dabie Mountains in Anhui Province. *Asian Herpetol Res* **8**:151–164.

Remya K, Ramachandran A, Jayakumar S, 2015. Predicting the current and future suitable habitat distribution of *Myristica dactyloides* gaertn. using maxent model in the Eastern Ghats, India. *Ecol Eng* **82**:184–188.

Rousset F, 2008. Genepop'007: a complete re-implementation of the genepop software for windows and linux. *Mol Ecol Resour* **8**:103–106.

Sheng HL, Cao KJ, Li WJ, Ma YQ, Ohtaishi N et al., 1992. *The Deer in China*. Shanghai: East China Normal University Press.

Shi Y, Liu S, Ye B, Liu C, Wang Z, 2008. *Concise Glacier Inventory of China*. Shanghai: Shanghai Popular Science Press.

Sievers M, Hale R, Parris KM, Swearer SE, 2018. Impacts of human-induced environmental change in wetlands on aquatic animals. *Biol Rev* **93**:529–554.

Slatkin M, 1977. Gene flow and genetic drift in a species subject to frequent local extinctions. *Theor Popul Biol* **12**:253–262.

Stanton JC, Shoemaker KT, Pearson RG, Akçakaya HR, 2015. Warning times for species extinctions due to climate change. *Glob Change Biol* **21**:1066–1077.

Storfer A, Murphy MA, Spear SF, Holderegger R, Waits LP, 2010. Landscape genetics: where are we now? *Mol Ecol* **19**:3496–3514.

Stucki S, Orozco-terWengel P, Forester BR, Duruz S, Colli L et al., 2017. High performance computation of landscape genomic models including local indicators of spatial association. *Mol Ecol Resour* **17**:1072–1089.

Sun ZL, Pan T, Wang H, Pang MJ, Zhang BW, 2016. Yangtze River, an insignificant genetic boundary in tufted deer *Elaphodus cephalophus*: the evidence from a first population genetics study. *PeerJ* **4**:e2654.

Sun ZL, Wang H, Zhou WL, Shi WB, Zhu WQ et al., 2019. How rivers and historical climate oscillations impact on genetic structure in Chinese muntjac *Muntiacus reevesi*? *Divers Distrib* **25**:116–128.

Swets JA, 1988. Measuring the accuracy of diagnostic systems. *Science* **240**: 1285–1293.

Taubmann J, Theissinger K, Feldheim KA, Laube I, Graf W et al., 2011. Modelling range shifts and assessing genetic diversity distribution of the montane aquatic mayfly *Ameletus inopinatus* in Europe under climate change scenarios. *Conserv Genet* **12**:503–515.

Templeton AR, 1998. Nested clade analyses of phylogeographic data: testing hypotheses about gene flow and population history. *Mol Ecol* **7**:381–397.

Teng HJ, Zhang YH, Shi CM, Mao FB, Cai WS et al., 2017. Population genomics reveals speciation and introgression between brown norway rats and their sibling species. *Mol Biol Evol* **34**:2214–2228.

Thomas CD, Cameron A, Green RE, Bakkenes M, Beaumont LJ et al., 2004. Extinction risk from climate change. *Nature* **427**:145–148.

Tian S, Lei SQ, Hu W, Deng LL, Li B et al., 2015. Repeated range expansions and inter-/postglacial recolonization routes of *Sargentodoxa cuneata* (Oliv.) rehd. Et wils.(Lardizabalaceae) in subtropical china revealed by chloroplast phylogeography. *Mol Phylogenet Evol* **85**:238–246.

Tremblay RL, Ackerman JD, 2001. Gene flow and effective population size in *Lepanthes* (Orchidaceae): a case for genetic drift. *Biol J Linn Soc* **72**:47–62.

Van Oosterhout C, Hutchinson WF, Wills DP, Shipley P, 2004. Micro-checker: software for identifying and correcting genotyping errors in microsatellite data. *Mol Ecol Notes* **4**:535–538.

VanDerWal J, Murphy HT, Kutt AS, Perkins GC, Bateman BL et al., 2013. Focus on poleward shifts in species' distribution underestimates the fingerprint of climate change. *Nat Clim Change* **3**:239–243.

Wang CC, Qian LF, Zhang CL, Guo WB, Pan T et al., 2017. A new species of *Rana* from the Dabie Mountains in eastern China (Anura, Ranidae). *ZooKeys* **724**:135–153.

Wang QS, 1990. *The Mammal Fauna of Anhui*. Hefei: Anhui Publishing House of Science and Technology.

Wang WM, Li CH, Shu JW, Chen W, 2019. Changes of vegetation in southern China. *Sci China Earth Sci* **49**:1308–1320.

Wei B, Wang RL, Hou K, Wang XY, Wu W, 2018. Predicting the current and future cultivation regions of *Carthamus tinctorius* L. Using maxent model under climate change in China. *Glob Ecol Conserv* **16**: e00477.

Wei SC, Li ZT, Momigliano P, Fu C, Wu H et al., 2020. The roles of climate, geography and natural selection as drivers of genetic and phenotypic differentiation in a widespread amphibian *Hyla annectans* (Anura: hylidae). *Mol Ecol* **29**:3667–3683.

Williams M, Dunkerley D, De Deckker P, Kershaw P, Chappell J et al., 1998. *Quaternary Environments*. London: Arnold.

Wisz MS, Hijmans RJ, Li J, Peterson AT, Graham CH et al., 2008. Effects of sample size on the performance of species distribution models. *Divers Distrib* **14**:763–773.

Yang C, Tang SH, Luo ZH, 2020. Distribution changes of Chinese skink *Eumeces chinensis* in China: the impacts of global climate change. *Asian Herpetol Res* **11**:132–138.

Yannic G, Pellissier L, Ortego J, Lecomte N, Couturier S et al., 2014. Genetic diversity in caribou linked to past and future climate change. *Nat Clim Change* **4**:132–137.

Yi YJ, Cheng X, Yang ZF, Zhang SH, 2016. Maxent modeling for predicting the potential distribution of endangered medicinal plant *H. riparia Lour* in Yunnan. *China. Ecol Eng* **92**:260–269.

Yuan ZY, Suwannapoom C, Yan F, Poyarkov NA Jr, Nguyen SN et al., 2016. Red river barrier and pleistocene climatic fluctuations shaped the genetic structure of *Microhyla fissipes* complex (Anura: microhylidae) in southern China and Indochina. *Curr Zool* **62**:531–543.

Zhang BW, Huang X, Pan T, Zhang L, Zhou WL et al., 2013. Systematics and species validity of the Dabieshan Pit Viper *Protobothrops dabieshanensis* Huang et al. 2012: evidence from a mitochondrial gene sequence analysis. *Asian Herpetol Res* **4**:282–287.

Zhang BW, Li M, Zhang ZJ, Goossens B, Zhu LF et al., 2007. Genetic viability and population history of the giant panda, putting an end to the "evolutionary dead end". *Mol Biol Evol* **24**:1801–1810.

Zhang H, Yan J, Zhang GQ, Zhou KY, 2008. Phylogeography and demographic history of Chinese black-spotted frog populations *Pelophylax nigromaculata*: evidence for independent refugia expansion and secondary contact. *BMC Evol Biol* **8**:21.

Zhao J, Shi Y, Wang J, 2011. Comparison between quaternary glaciations in china and the marine oxygen isotope stage (MIS): an improved schema. *Acta Geogr Sin* **66**:867–884.

Zhao SC, Zheng PP, Dong SS, Zhan XJ, Wu Q et al., 2013. Whole-genome sequencing of giant pandas provides insights into demographic history and local adaptation. *Nat Genet* **45**:67–71.

Zhao Y, Yu ZC, 2012. Vegetation response to holocene climate change in east asian monsoon-margin region. *Earth-Sci Rev* **113**:1–10.

Zhao YX, Yang J, Lv FH, Hu XJ, Xie XL et al., 2017. Genomic reconstruction of the history of native sheep reveals the peopling patterns of nomads and the expansion of early pastoralism in East Asia. *Mol Biol Evol* **34**: 2380–2395.

Zheng YH, Zhang Y, Shao XM, Yin ZY, Zhang J, 2012. Temperature variability inferred from tree-ring widths in the dabie mountains of subtropical central China. *Trees* **26**:1887–1894.

Zhou XM, Meng XH, Liu ZJ, Chang J, Wang BS et al., 2016. Population genomics reveals low genetic diversity and adaptation to hypoxia in snub-nosed monkeys. *Mol Biol Evol* **33**:2670–2681.

Zhou Y, Qiu G, Guo D, 1991. Changes of permafrost in China during Quaternary. In: Liu TS, editor. *Quaternary Geology and Environment in China*. Beijing: Science Press. 86–94.